

AFRL-RW-EG-TP-2008-7419

EXPERIMENTAL AND THEORETICAL INVESTIGATION OF THE HIGH-PRESSURE BEHAVIOR OF CONCRETE

Martin J. Schmidt (AFRL/RWAC)
Mark L. Green (AFRL/RWMW)
Air Force Research Laboratory
Eglin AFB, FL 32542

Oana Cazacu (UF/Reef)
Department of Mechanical
and Aerospace Engineering
University of Florida REEF
Shalimar, FL 32579



SEPTEMBER 2008

JOURNAL ARTICLE

© 2008 John Wiley & Sons, Ltd. [doi: 10.1002/nag.700]

This article has been published online in the International Journal for Numerical and Analytical Methods in Geomechanics, 6 March 2008, and is copyrighted.

One or more of the authors is a U.S. Government employee working within the scope of their position; therefore, the U.S. Government is joint owner of the work, and has the right to copy, distribute, and use the work by, or on behalf of, the U.S. Government. All other rights are reserved by the copyright owner.

This paper is published in interest of the scientific and technical exchange. Publication of this report does not constitute approval or disapproval of the ideas or findings.

DISTRIBUTION A: Approved for public release; distribution unlimited.
Approval Confirmation AAC/PA # 04-11-07-243; dated 11 April 2007.

AIR FORCE RESEARCH LABORATORY, MUNITIONS DIRECTORATE

■ Air Force Material Command ■ United States Air Force ■ Eglin Air Force Base

REPORT DOCUMENTATION PAGE				<i>Form Approved OMB No. 0704-0188</i>	
<small>The public reporting burden for this collection of information is estimated to average 1 hour per response, including the time for reviewing instructions, searching existing data sources, gathering and maintaining the data needed, and completing and reviewing the collection of information. Send comments regarding this burden estimate or any other aspect of this collection of information, including suggestions for reducing the burden, to Department of Defense, Washington Headquarters Services, Directorate for Information Operations and Reports (0704-0188), 1215 Jefferson Davis Highway, Suite 1204, Arlington, VA 22202-4302. Respondents should be aware that notwithstanding any other provision of law, no person shall be subject to any penalty for failing to comply with a collection of information if it does not display a currently valid OMB control number.</small>					
PLEASE DO NOT RETURN YOUR FORM TO THE ABOVE ADDRESS.					
1. REPORT DATE (DD-MM-YYYY)		2. REPORT TYPE		3. DATES COVERED (From - To)	
4. TITLE AND SUBTITLE				5a. CONTRACT NUMBER	
				5b. GRANT NUMBER	
				5c. PROGRAM ELEMENT NUMBER	
6. AUTHOR(S)				5d. PROJECT NUMBER	
				5e. TASK NUMBER	
				5f. WORK UNIT NUMBER	
7. PERFORMING ORGANIZATION NAME(S) AND ADDRESS(ES)				8. PERFORMING ORGANIZATION REPORT NUMBER	
9. SPONSORING/MONITORING AGENCY NAME(S) AND ADDRESS(ES)				10. SPONSOR/MONITOR'S ACRONYM(S)	
				11. SPONSOR/MONITOR'S REPORT NUMBER(S)	
12. DISTRIBUTION/AVAILABILITY STATEMENT					
13. SUPPLEMENTARY NOTES					
14. ABSTRACT					
15. SUBJECT TERMS					
16. SECURITY CLASSIFICATION OF:			17. LIMITATION OF ABSTRACT	18. NUMBER OF PAGES	19a. NAME OF RESPONSIBLE PERSON
a. REPORT	b. ABSTRACT	c. THIS PAGE			19b. TELEPHONE NUMBER (Include area code)

Experimental and theoretical investigation of the high-pressure behavior of concrete

Martin J. Schmidt^{1,*}, Oana Cazacu² and Mark L. Green¹

¹*Air Force Research Laboratory, Eglin AFB, FL 32542, U.S.A.*

²*Department of Mechanical and Aerospace Engineering, University of Florida REEF, Shalimar, FL 32579, U.S.A.*

SUMMARY

The results of an experimental study aimed at characterizing the behavior of concrete for high confining pressures (up to 500 MPa) are reported. The main characteristics of the response under deviatoric conditions are quasi-linearity in the elastic regime, stress-path dependency, and gradual change from compressibility to dilatancy under increasing deviatoric stress. By performing the cyclic triaxial compression tests with several load–creep–unload and reload cycles, the time influence on the overall behavior was detected. Further, whether the main features of the observed behavior can be described within the framework of elastic/viscoplasticity theory was investigated. For this purpose, Cristescu's (*Rock Rheology*, Kluwer Academic Publishers: The Netherlands, 1989) approach was used. It was shown that the proposed elastic/viscoplastic model captures the main features of concrete behavior at high pressures. Copyright © 2008 John Wiley & Sons, Ltd.

Received 3 August 2007; Revised 30 November 2007; Accepted 14 January 2008

KEY WORDS: concrete; high confinement; compressibility; viscoplasticity

Dedicated to Professor N. D. Cristescu in recognition of his major contributions to geomechanics

1. INTRODUCTION

A rather significant literature exists on the quasi-static mechanical response of cementitious materials and geomaterials. However, most of the experimental results are obtained using triaxial cells and concern the response under moderate confining pressures, i.e. up to approximately 100 MPa (see, for example, [1–4], etc.). True triaxial compression test results reported are for the same range of pressures (see, for example, [4, 5]). Bazant *et al.* [6] have developed an oedometric-type test that allows characterization of the response at high pressures. A cylindrical specimen (height 44.4 mm,

*Correspondence to: Martin J. Schmidt, Air Force Research Laboratory, Eglin AFB, FL 32542, U.S.A.

†E-mail: martin.schmidt@egli.af.mil

diameter 18.8 mm) is placed in a very rigid hollow plate, which prevents lateral deformation, and is subjected to compression parallel to its vertical axis. The major limitations are related to the size of the specimens and accurate evaluation of frictional effects. Bourlion *et al.* [7] have extended this testing method to allow testing of concrete with aggregate sizes up to 16 mm at levels of mean pressure of about 600 MPa. These authors have also reported true hydrostatic test results on small mortar size specimens.

There is a large body of literature on modeling the behavior of cementitious materials. For moderate levels of pressure, the non-linearity of the response is mainly due to damage by micro- and meso-crack's growth. Major developments have occurred over the past decades in modeling the behavior at continuum level. Continuum damage models of various degrees of complexity have been proposed (for comprehensive reviews of the main contributions, see [8, 9]). For higher levels of pressure (mean stress or confinement), the behavior is more ductile and plasticity models (e.g. [10, 11]) as well as coupled damage-plasticity models ([12–16], etc.) are more appropriate.

To model time effects on the non-linear behavior of cementitious materials, a very large number of models developed for inviscid behavior have been extended in the rate-dependent range using the overstress concept (see, [17]). Thus, the expressions of the constitutive functions (i.e. yield function, plastic potential) used in these rate-sensitive models are the same as the ones used to describe inviscid behavior. In contrast, the approach introduced by Cristescu (see, for instance, [4]) is to determine the specific expressions of the yield function and viscoplastic potential for a given material directly from creep data. This allows describing both compressibility and dilatancy by a unique continuous yield function and viscoplastic potential, respectively.

In this paper, we present the results of an experimental investigation into the effects of high confinement on the deformation and strength of a concrete material. By performing cyclic triaxial compression (CTC) tests with several load–creep–unload and reload cycles, the time influence on the overall behavior was detected. Based on these data, an elastic/viscoplastic model that captures compressibility, dilatancy, and strain rate effects has been developed. The structure of this model and a procedure for determining the expressions of the constitutive functions and material parameters based on a minimal set of data are given in Section 3. We conclude by presenting comparison between model simulations and data.

2. EXPERIMENTAL STUDY

The aim of this experimental study is to extend the existing database on the deformation and failure of concrete by investigating the behavior over a range of pressures characteristic of impact events. Of particular interest was the influence of very high confining pressure (up to 500 MPa) on the material's deformation and strength. Thus, the experimental program included (a) quasi-static hydrostatic compression tests from which the increase in the compressibility of the material and an estimate of the compaction properties over the range pressures encountered in impact events can be inferred, (b) quasi-static CTC tests under lateral confining pressure, σ_3 , ranging from 50 to 500 MPa, based on which the effect of loading history on the response and the importance of short-term time effects on the behavior can be determined. A total of 21 tests were conducted at the U.S. Army Corps of Engineer Engineering Research and Development Center, Waterways Experiment Station (WES) in Vicksburg, Mississippi.

2.1. Material studied

The mixture proportions and resulting basic properties of the concrete studied are given in Table I. The concrete is a mixture of Portland cement, chert aggregates (fine and coarse), fly ash, water, and water-reducing admixture. The uniaxial compressive and tension strengths at 28 days were 45.6 and 3.13 MPa, respectively. The test results indicate that under uniaxial compression, the material exhibits typical brittle behavior.

2.2. Specimen preparation and quasi-static test instrumentation

Prior to each test, the prepared specimen was weighed, carefully measured, and ultrasonic measurements (P- and S-wave velocities) were taken. For all tests, the specimens had a nominal height of 110 mm and a diameter of 50 mm. Because of the inherent heterogeneity of the material and the high-pressure range in which it was tested, instrumentation with strain gages was found unreliable. Instead, to measure the displacement between the top and the base caps (i.e. determine the axial deformation of the specimen), two linear variable differential transformers (LVDTs) mounted vertically on the instrumentation stand and positioned 180° apart were used. The radial deflection was measured using two LVDTs, which were connected to two small steel footings mounted diametrically (180° apart) at the mid-height of the specimen (see Figure 1). A gypsum paste was used to patch all voids. Subsequent to patching of the voids, the specimen was encased in a latex membrane, and this membrane was then surrounded by a layer of putty-like material. The putty served the function of self-sealing any potential punctures of the inner membrane. A second latex membrane was then applied over the putty and the membrane was coated with a sealant to prevent its degradation by the petroleum-based hydraulic fluid.

The axial load was provided by an 8.9 MN loading machine (Secodyne) coupled with 600-MPa-capacity pressure cell (see the schematic diagram in Figure 2). The loading rate/profile was computer programmable, allowing for precise control of the experiments under load, displacement, or strain control.

2.3. Experimental results

A triaxial compression test is generally conducted in two phases: a hydrostatic compression phase and a deviatoric phase. During the hydrostatic phase, the specimen is subjected to isotropic compression, while measurements of the axial and radial deformations are made. The deviatoric

Table I. Ingredients and mixture proportions for WES5000 concrete.

Item	Mixture proportions, saturated surface-dry
Type I Portland cement	264.0 kg/m ³
Flyash	55.8 kg/m ³
9.5 mm local unprocessed chert coarse aggregate	1037.6 kg/m ³
Local unprocessed chert fine aggregate	840.7 kg/m ³
Water	145.9 kg/m ³
Water-reducing admixture '300N'	0.65 l/m ³
High-range water reducing admixture 'Rheobuild 716'	1.6 l/m ³



Figure 1. Spring-arm lateral LVDT mounted on test specimen.

phase of the test is conducted after the desired confining pressure has been reached during the hydrostatic phase. While holding the desired lateral confining pressure constant, the axial load is increased until the specimen fails. As an example, the pressure *vs* volumetric data obtained from the hydrostatic phase of a CTC test under 200 MPa confining pressure are presented in Figure 3. In order to evaluate the bulk modulus, an unloading–reloading cycle was performed at 100 MPa. Note the significant hysteresis displayed, which clearly makes the determination of the bulk modulus highly imprecise.

To determine the elastic properties with accuracy, it is necessary to ensure a good separation between viscous effects and unloading. One way of accomplishing this is to hold the stress constant before each unloading/reloading cycle such as to allow the material to creep. The duration of the creep stage (time interval in which the load is kept constant) is usually determined by monitoring the rate of change of the strains. When the strain rate approaches zero, i.e. the material reaches by creep a quasi-stable state, unloading is conducted. More details concerning this experimental procedure and its application to a variety of geologic materials can be found in Cristescu and

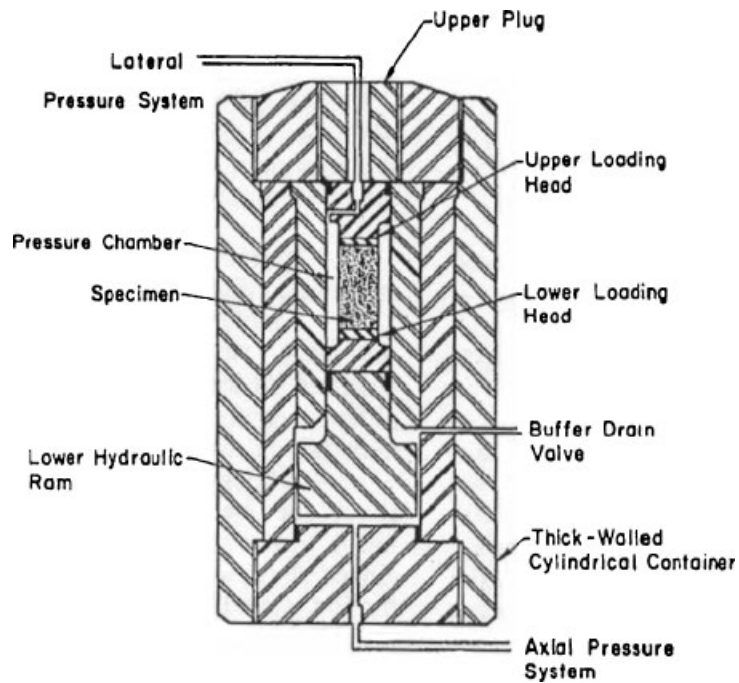


Figure 2. Section through triaxial pressure cell.

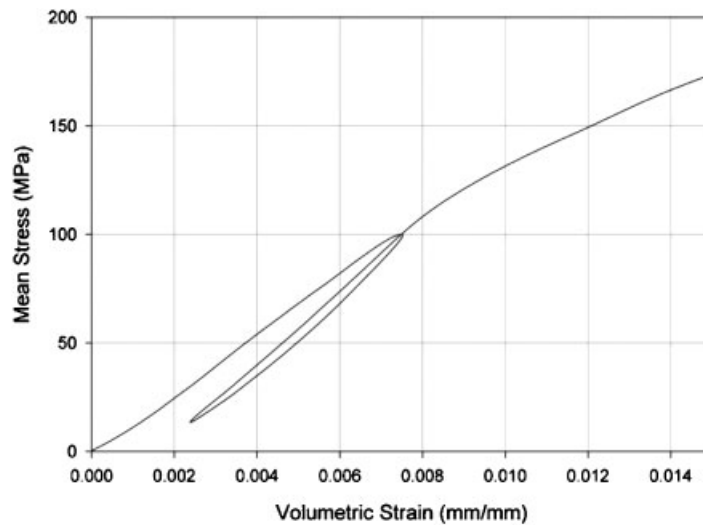


Figure 3. Mean stress–volumetric strain data from a hydrostatic cyclic test on concrete.

Hunsche [4]. This step-wise loading procedure was used for the hydrostatic phase of each CTC test conducted. As an example, the results of a hydrostatic test up to 500 MPa are shown in Figure 4.

The close agreement between the axial and radial gage measurements indicates that the material is isotropic. The test consisted of seven loading–creep–unloading–reloading cycles. For each cycle, prior to unloading, the pressure was held constant for 30 min. Then, partial unloading and further reloading were performed. In Figure 5, the volumetric strain rate *vs* time data corresponding to the

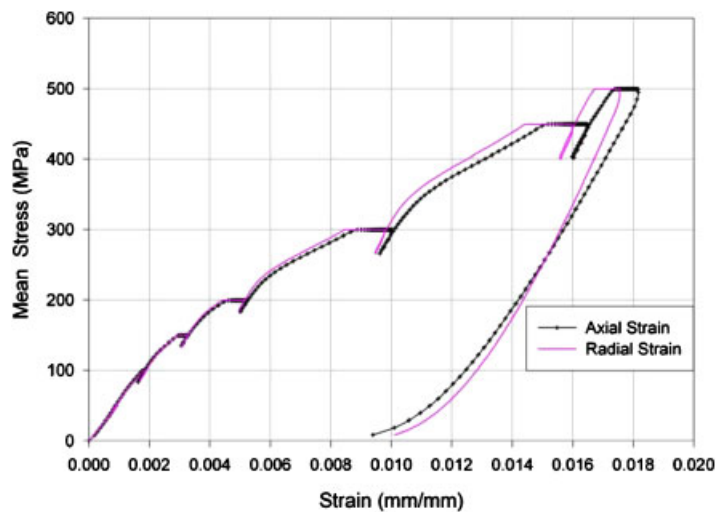


Figure 4. Mean stress–volumetric strain data from a hydrostatic test up to 500 MPa conducted following a step-wise loading/creep/partial unloading procedure.

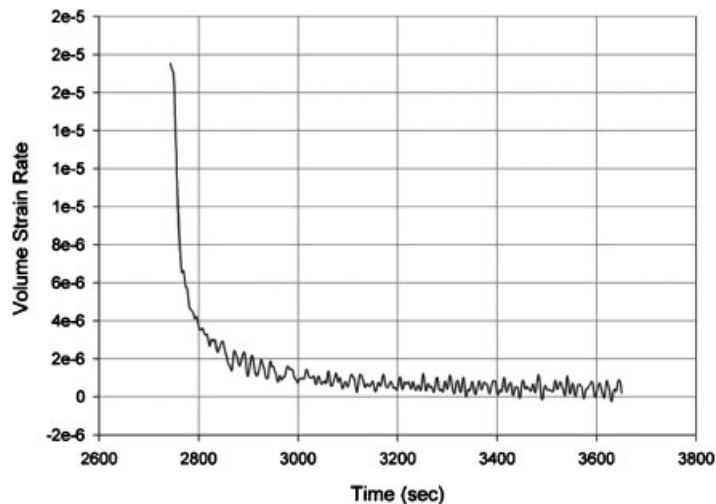


Figure 5. Volumetric strain rate *vs* time from the second cycle (unload at 100 MPa) of a hydrostatic test up to 500 MPa.

second cycle (unloading at 100 MPa) are presented. It can be seen that within the duration of the creep stage, the rate of change of the volumetric strain with time approached zero. In Figure 6, the pressure–strain curve corresponding to the second creep–loading–unloading–reloading cycle is shown. Note that very little hysteresis is present, and the slope of the quasi-linear part of the unloading curve coincides with the slope of the quasi-linear part of the reloading curve. The bulk modulus, K , corresponding to several pressure levels was evaluated from the slopes of the quasi-linear part of the unloading curves of pressure vs volumetric strain. The bulk modulus was found to increase with the applied pressure from $K = 23.24$ GPa (second cycle) to $K = 28.76$ GPa (last cycle). The reduction in porosity at the end of the test (i.e. at 0.5 GPa) is approximately 2.5%. Figure 7 shows the principal stress–strain data from the deviatoric phase of a CTC test conducted at $\sigma_3 = 375$ MPa confining pressure following a step-wise loading procedure. Note that the material exhibits irreversible time-dependent behavior. The stress vs volumetric strain curve also shows a highly non-linear volume response, with the onset of dilatancy being very close to failure. The same trends have been observed in all the tests conducted. Figure 8 shows a comparison of the stress–strain data from the deviatoric phase of CTC tests at confining pressures of 200, 300, and 450 MPa, whereas in Figure 9 presents the strength values determined in the same tests. It is clearly seen that higher confinement produces higher yield stress, increased hardening, and increased strength.

From the test results, we can conclude that for high pressures, the material displays irreversible time-dependent properties. On the other hand, the analysis of the variation of Young's modulus with pressure (see Figure 10) shows that for specific levels of radial confinement, E is decreasing with the mean stress, which is indicative of damage. Modeling of damage and damage couplings with plasticity and viscous effects is beyond the scope of this paper. We will model only the main features of the behavior, i.e. time effects on the plastic behavior within the framework of viscoplasticity.

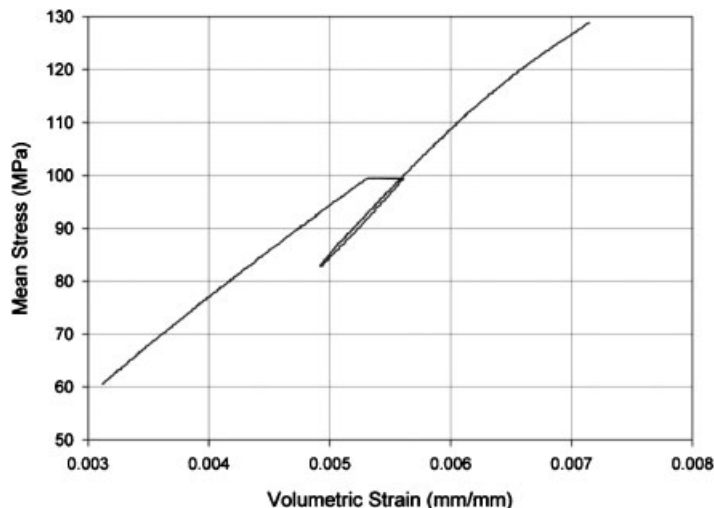


Figure 6. Mean stress–volumetric strain data from the second cycle (unload at 100 MPa) of a hydrostatic test up to 500 MPa.

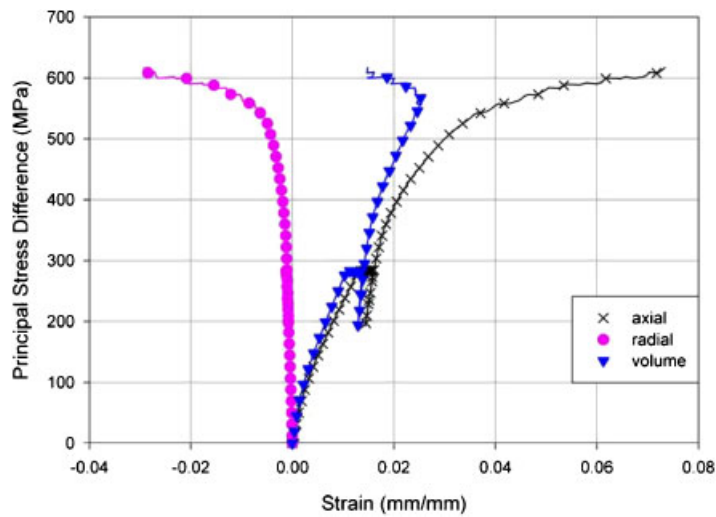


Figure 7. Stress–strain data from the deviatoric phase of a cyclic triaxial compression test at a confining pressure of 375 MPa.

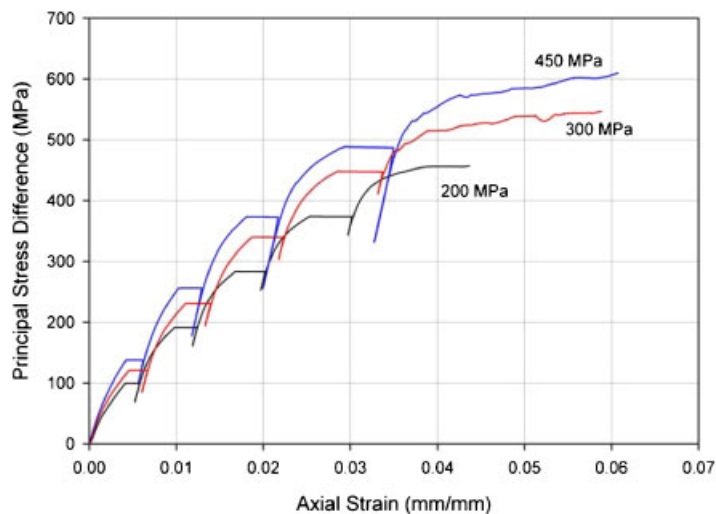


Figure 8. Stress–strain data from the deviatoric phase of cyclic triaxial compression tests at confining pressures of 200, 300, and 450 MPa.

3. ELASTIC–VISCOPLASTIC MODEL DEVELOPMENT

The most widely used approach to model coupling between plastic and viscous effects on the behavior of geological or cementitious materials is that proposed by Perzyna [17] (see also [18]). The basic assumption is that the viscous properties of materials become manifest only after the

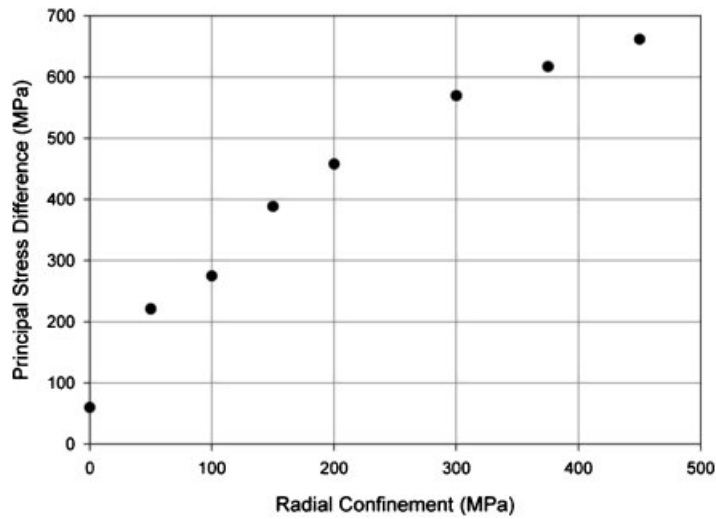


Figure 9. Ultimate strength as a function of confining pressure.

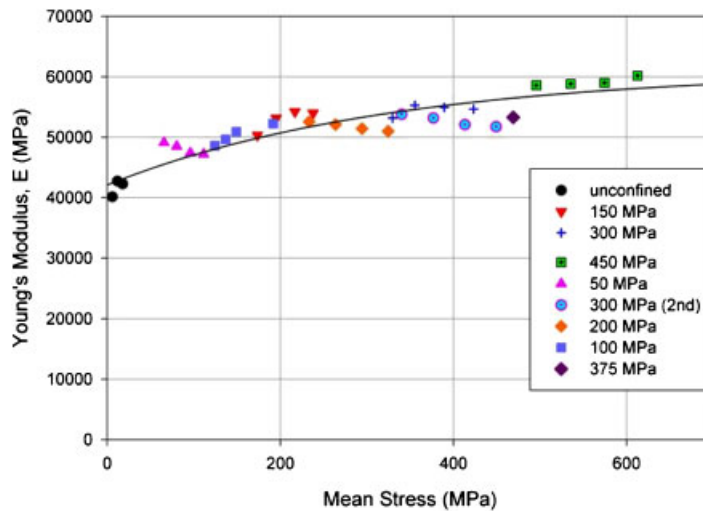


Figure 10. Comparison between theoretical and experimental variations of Young's modulus E with the mean stress.

passage to the plastic state. The expressions of the constitutive functions (yield function, viscoplastic potential) are the same as the ones used to describe the elastic/plastic, time-independent behavior. In this paper, we will use the elastic/viscoplastic modeling framework proposed by Cristescu (see, for instance, [4]), i.e. the mathematical expressions of the constitutive functions are *a priori* unknown and will be determined from the experimental data (creep test results). We begin by briefly reviewing the general elastic/viscoplastic framework and then present the simplifying assumptions

made in order to obtain a reasonably simple mathematical model for the given material. It is assumed that the material is homogeneous and isotropic. The reference configuration is the actual configuration. The displacements and material rotations are assumed to be small. Thus, the strain rate $\dot{\boldsymbol{\varepsilon}}$ can be decomposed additively into an elastic part, $\dot{\boldsymbol{\varepsilon}}^E$, and an irreversible part, $\dot{\boldsymbol{\varepsilon}}^I$, i.e.

$$\dot{\boldsymbol{\varepsilon}} = \dot{\boldsymbol{\varepsilon}}^E + \dot{\boldsymbol{\varepsilon}}^I \quad (1)$$

The elastic component of the strain rate is given by

$$\dot{\boldsymbol{\varepsilon}}^E = \frac{\dot{\boldsymbol{\sigma}}}{2G} + \left(\frac{1}{3K} - \frac{1}{2G} \right) \dot{p} \mathbf{I} \quad (2)$$

where the dot stands for the derivative with respect to time, G and K are the shear and bulk moduli, respectively, \mathbf{I} is the second-order identity tensor, and p is the mean stress (i.e. $p = \text{tr}(\boldsymbol{\sigma})/3$). No assumption concerning the existence of a viscoplastic potential is made. Thus, the irreversible strain rate is considered to be given by an overstress-type law of the form:

$$\dot{\boldsymbol{\varepsilon}}^I = k_T \left\langle 1 - \frac{W(t)}{H(\boldsymbol{\sigma})} \right\rangle (\boldsymbol{\sigma}) \quad (3)$$

where t is the actual time and $W(t)$ is the irreversible stress work per unit volume. The only restriction imposed on the tensor-valued $N(\boldsymbol{\sigma})$, which defines the orientation of the viscoplastic strain rate, is to be isotropic (see [19]). In (3), the symbol $\langle \cdot \rangle$, known as the Macaulay bracket, denotes $\langle x \rangle = (x + |x|)/2$ and k_T is a viscosity coefficient. Thus, there is viscoplastic flow if and only if $H(\boldsymbol{\sigma}) > W(t)$. Only transient creep is modeled. From (3) it follows that the deformation due to transient creep stops after a certain finite time interval and stabilization takes place, the equation for the stabilization boundary for creep being

$$H(\boldsymbol{\sigma}) = W(t) \quad (4)$$

Note that this choice of hardening variable is appropriate for the description of the behavior of concrete because it captures both the shear and the volumetric inelastic effects. Indeed, $W(t)$ can be decomposed into two terms:

$$W(t) = \int_0^t \boldsymbol{\sigma}(t) : \dot{\boldsymbol{\varepsilon}}^I(t) dt = W_H(t) + W_D(t) \int_0^t p(t) \dot{\varepsilon}_v^I(t) dt + \int_0^t \boldsymbol{\sigma}'(t) : \dot{\boldsymbol{\varepsilon}}'(t) dt \quad (5)$$

where $W_H(t)$ is the energy related to irreversible volume change that is stored during compaction or released during dilatancy (volumetric expansion) of the material, and $W_D(t)$ is always positive and represents the energy input needed for change in shape. In (5), $\dot{\varepsilon}_v^I(t)$ is the irreversible volumetric strain rate and $\boldsymbol{\sigma}'(t)$ is the stress deviator.

The first step in the development of the elastic–viscoplastic model for the material studied is the description of the elastic behavior. For each CTC test conducted, Young's modulus, E , and the bulk modulus, K , were evaluated from the slopes of the quasi-linear parts of the unloading–reloading cycles performed at the end of each of the creep steps. We also estimated the corresponding Poisson ratio, ν . As it is the case with most rocks, soils, and cementitious materials, the elastic moduli are stress dependent. Thus, the stress–strain relationship (2) is hypoelastic in the sense of Truesdell [20]. The necessary and sufficient conditions for an isotropic material with stress-dependent elastic moduli to have a conservative response in the elastic regime were established by Loret [21]. It was

shown that the choice of the laws of variation of the elastic moduli with the stress state cannot be arbitrary. The laws of variation should be expressible in terms of the stress invariants: the mean stress p , and the second invariant of the stress deviator $q = \sqrt{\frac{3}{2}\text{tr}(\boldsymbol{\sigma}')^2}$. An analysis of the variation in Young's modulus with pressure indicates a global increase in E with increasing p . However, for certain levels of radial confinement, a decrease in E , which is indicative of damage, is observed. Modeling of damage and damage couplings with plasticity and viscous effects is beyond the scope of this paper. We model only the increase in E with pressure by considering the following law of variation:

$$E(p) = E^\infty - b \exp(-p/c) \quad (6)$$

In (6), E^∞ is the asymptotic limit towards which E tends as the pressure becomes very large, ($p \rightarrow \infty$), i.e. the value of the Young modulus corresponding to a fully compacted state. Good overall agreement with all the available data is obtained for $E^\infty = 61$ GPa, $b = E^\infty - E|_{p=0} = 18.92$ GPa, and $c = b(dE/dp|_{p=0}) = 0.33$ MPa (see Figure 10). We consider $\nu = 0.175$, a value that corresponds to the mean of the experimental values from all tests (see Figure 11), and calculate K from the elasticity relationship:

$$K = \frac{E}{3(1-2\nu)} \quad (7)$$

Several factors entered into assuming a constant value of the Poisson ratio. First, for the sake of simplicity, it was seen advisable to limit the number of coefficients involved in the model. Also, due to the overall higher level of confidence in the axial measurements, it was found best to approximate the experimental variation of E with the mean stress rather than to approximate the experimental evolution of the bulk modulus. Furthermore, a value of 0.175 for the Poisson ratio is

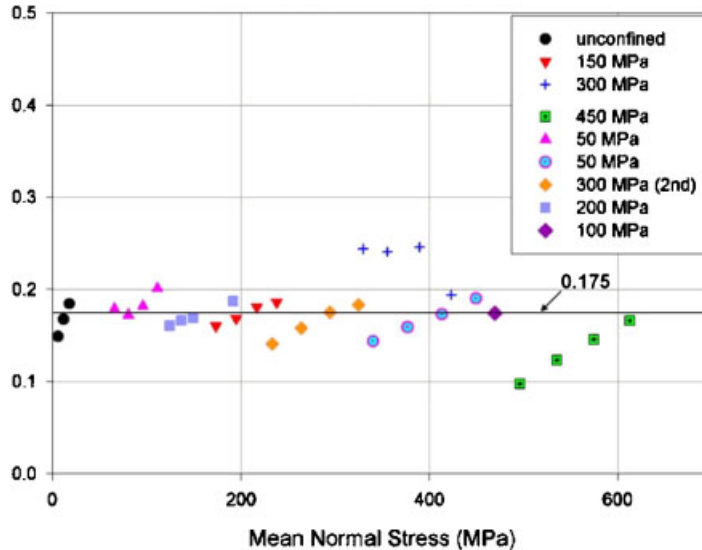


Figure 11. Experimental variation of Poisson's ratio with the mean stress.

well within the range of values typically observed for concrete (see [22]). Note that Equation (7) with E given by (6) approximates well the experimental variation of the bulk modulus K with the mean stress (see Figure 12). The material being isotropic, the yield function, H , depends on $\boldsymbol{\sigma}$ through its invariants. The experimental data available were obtained from CTC tests in which only two principal stresses can be varied and measured independently, i.e. σ_1 and $\sigma_2 = \sigma_3$. The effect of the third invariant of stress cannot be inferred without data for which all three principal stresses can be varied independently. That is why we assume that $H(\boldsymbol{\sigma}) = H(p, q)$, where $q = \sqrt{\frac{3}{2} \text{tr}(\boldsymbol{\sigma}')^2}$ is the second invariant of the stress deviator $\boldsymbol{\sigma}'$. To determine the specific expression of $H(p, q)$ based on CTC results, we adopt the procedure proposed by Cristescu [3] (see also [4]). Thus, we assume that $H(p, q)$ can be expressed as

$$H(p, q) = H_H(p) + H_D(p, q) \quad (8)$$

such that

$$H_D(p, 0) = 0 \quad (9)$$

where $H_H(p) = W_H$ and $H_D(p, q) = W_D$, W_H and W_D being the volumetric and deviatoric parts of the irreversible stress work at creep stabilization. Thus, in order to determine $H_H(p)$, we calculated the irreversible stress work corresponding to creep stabilization according to the following equation:

$$W_H(t_H) = \int_0^{t_H} p(t) \dot{\varepsilon}_v^I(t) dt \quad (10)$$

using data from the hydrostatic phase of CTC tests at 150, 300, 450, and 500 MPa confinement, respectively. In (10), $\dot{\varepsilon}_v^I$ is the irreversible volumetric strain and t_H corresponds to the end of the hydrostatic phase of a CTC test. Next, we plotted the obtained values of $W_H(t)$ as a function of p . Note that W_H increases monotonically with the mean pressure. However, for very high levels

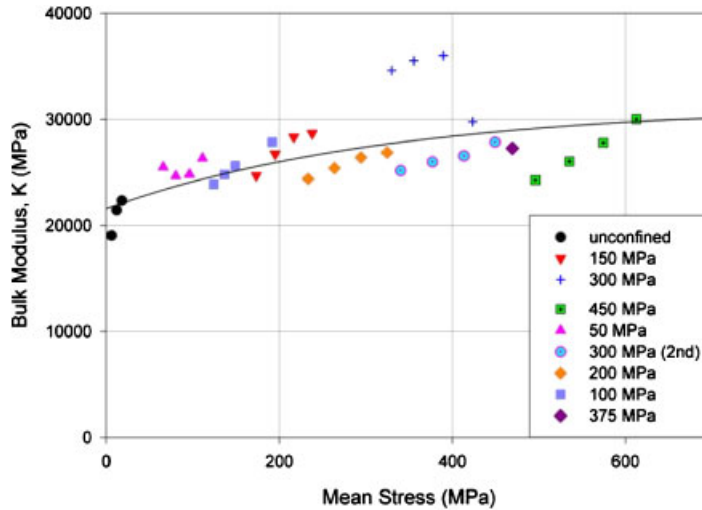


Figure 12. Comparison between theoretical and experimental variations of the bulk modulus K with the mean stress.

of pressures, the W_H vs p curve should reach a plateau, which corresponds to a state where all the micro-cracks and pores are closed (i.e. material is fully compacted). This plateau obviously lies beyond the hydrostatic pressure limit of the equipment available. An approximate value may be inferred from post-test observations of the density distribution of concrete targets impacted at conventional striking velocities. Indeed, X-ray measurements show that at about 2–3 projectile radii around the penetration tunnel, the target material is fully compacted. Assuming that the pressure corresponding to fully compacted state is of the same order of magnitude as the penetrator strength, the plateau is at about 1 GPa (see [23]). The experimental W_H data at stabilization were approximated with the function:

$$H_H(p) = \frac{a_h}{2c_h} \left[2d_h \ln \left(\exp \left(\frac{2p+c_h}{2d_h} \right) + \exp \left(\frac{b_h}{d_h} \right) \right) - 2d_h \ln \left(\exp \left(\frac{p}{d_h} \right) + \exp \left(\frac{2b_h+c_h}{2d_h} \right) \right) + c_h \right] + e_h \quad (11)$$

with $a_h = 12.6$ MPa, $b_h = 364.28$ MPa, $c_h = -365$ MPa, $d_h = 30.7$ MPa, and $e_h = 0.003$ MPa. Figure 13 shows the values of the irreversible volumetric stress work obtained from experimental data in the hydrostatic tests and the approximating function.

Similarly, $H_D(p, q)$ is determined from the data obtained in the deviatoric phase of the CTC tests. The irreversible stress work is computed using

$$W_D(T) = \int_{t_H}^T \sigma_3(t) \dot{\epsilon}_v^I(t) dt + \int_{t_H}^T q(t) \dot{\epsilon}_1^I(t) dt, \quad t \geq t_H \quad (12)$$

where t_H represents the beginning of the deviatoric part of the test and T corresponds to the end of the creep stage. Figure 14 shows the experimental values of W_D obtained from several CTC

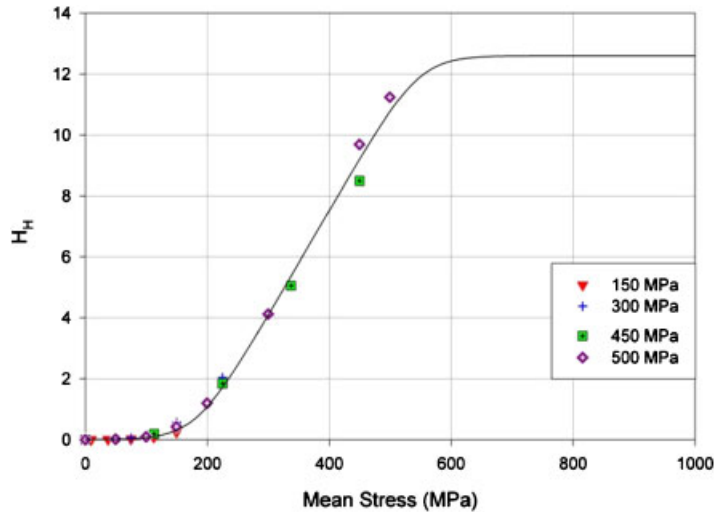


Figure 13. Stabilization boundary as a function of the mean stress (solid line); experimental values of the irreversible stress work at creep stabilization for various confining pressures (symbols).

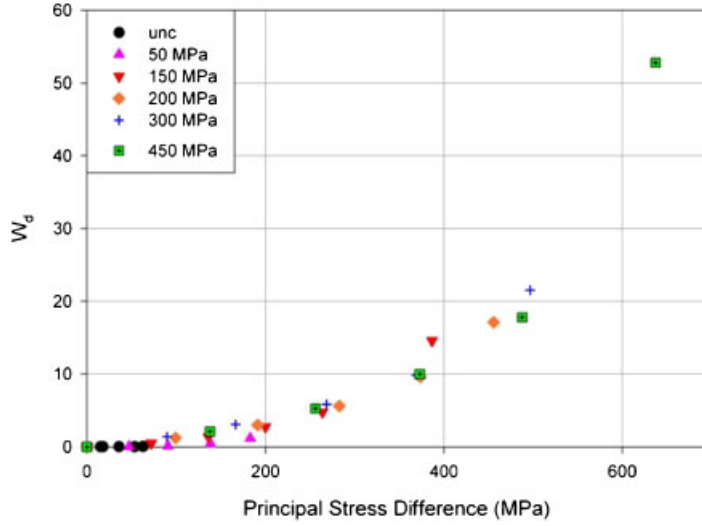


Figure 14. Experimental values of the irreversible stress work at stabilization as calculated based on the results in the deviatoric phase of several CTC tests.

tests. At any given confining pressure, the data trend is the same, i.e. initially linear, eventually curving upward, and asymptoting towards infinity as the specimen approaches failure.

A function that well approximates the data is

$$H_D(p, q) = d_0 q + d_1 q^2 + d_2 \exp(d_3 q^2) - d_2 \quad (13)$$

The coefficients d_i depend on the confining pressure σ_3 and are expressed as

$$d_0(\sigma_3) = d_{0a} \cdot (1 - \exp(d_{0b} \sigma_3)) \quad (14)$$

$$d_1(\sigma_3) = d_{1a} \cdot (1 - \exp(d_{1b} \sigma_3)) \quad (15)$$

$$d_2(\sigma_3) = d_{2a} + d_{2b} \cdot (1 - \exp(d_{2c} \sigma_3)) \quad (16)$$

$$d_3(\sigma_3) = \frac{d_{3a}}{1 + d_{3a} \cdot d_{3b} \cdot \sigma_3} \quad (17)$$

with $d_{0a} = 0.0141$, $d_{0b} = -0.0075$, $d_{1a} = 4.08 \times 10^{-5} \text{ MPa}^{-1}$, $d_{1b} = -0.005 \text{ MPa}^{-1}$, $d_{2a} = 1.6 \times 10^{-4} \text{ MPa}$, $d_{2b} = 0.0564 \text{ MPa}$, $d_{2c} = -0.0082 \text{ MPa}^{-1}$, $d_{3a} = 0.00135 \text{ MPa}^{-1}$, and $d_{3b} = 175.26$. As an example, a comparison between the approximating function and the experimental results corresponding to 200 MPa confining pressure is shown in Figure 15. The results of this test were not used in the determination of (13). A very good agreement is observed.

According to the constitutive equation (3), the tensorial function $N(\boldsymbol{\sigma})$ governs the orientation of the irreversible strain rate, $\dot{\boldsymbol{\varepsilon}}^I$. For an isotropic material, $N(\boldsymbol{\sigma})$ must satisfy the invariance requirement

$$N(Q\boldsymbol{\sigma}Q^T) = QN(\boldsymbol{\sigma})Q^T \quad (18)$$

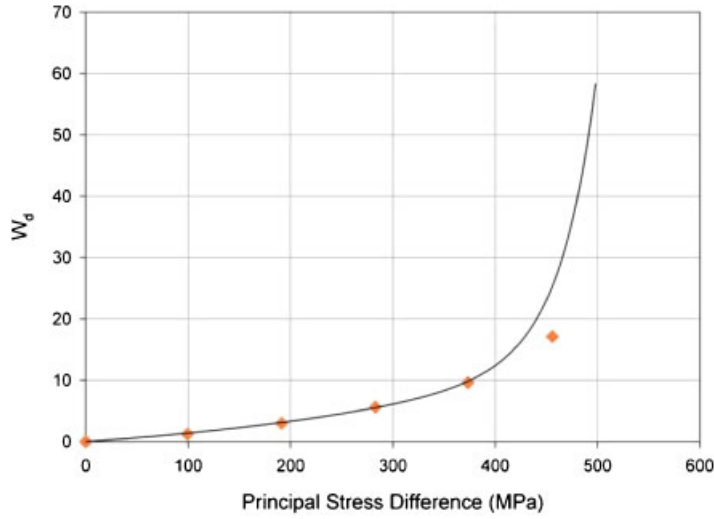


Figure 15. Comparison between theoretical and experimental variations of the irreversible stress work as a function of the deviatoric stress at a confining pressure of 200 MPa.

for any orthogonal transformation Q . From classical results regarding the representation of isotropic tensor functions (e.g. [24]), it follows that $N(\boldsymbol{\sigma})$ can be represented as

$$N(\boldsymbol{\sigma}) = N_1 \mathbf{I} + N_2 \boldsymbol{\sigma} + N_3 \boldsymbol{\sigma}^2 \quad (19)$$

where N_1 , N_2 , and N_3 are scalar-valued functions of all stress invariants. Third invariant dependence cannot be inferred without data for which all three principal stresses are distinct, and such data are not discussed in this paper. Thus, we consider $N(\boldsymbol{\sigma})$ to be of the form

$$N(\boldsymbol{\sigma}) = N_1(p, q) \mathbf{I} + N_2(p, q) \frac{\boldsymbol{\sigma}'}{q} \quad (20)$$

Hence,

$$\dot{\boldsymbol{\varepsilon}}^I = k_T \left\langle 1 - \frac{W(t)}{H(\boldsymbol{\sigma})} \right\rangle \left\{ N_1(p, q) \mathbf{I} + N_2(p, q) \frac{\boldsymbol{\sigma}'}{q} \right\} \quad (21)$$

It follows that for CTC loading:

$$k_T N_1(p, q) = \frac{\dot{\varepsilon}_v^I}{3 \left\langle 1 - \frac{W(t)}{H(\boldsymbol{\sigma})} \right\rangle} \quad (22)$$

$$k_T N_2(p, q) = \frac{|\dot{\varepsilon}_1^I - \dot{\varepsilon}_3^I|}{\left\langle 1 - \frac{W(t)}{H(\boldsymbol{\sigma})} \right\rangle} \quad (23)$$

where $\dot{\varepsilon}_1^I$ and $\dot{\varepsilon}_3^I$ denote the axial and radial irreversible strain rates, respectively. Equation (22) indicates that $N_1(p, q)$ models the irreversible volumetric response, whereas from Equation (23)

it follows that $N_2(p, q)$ describes the irreversible shear response. We assume that $k_T N_1$ can be expressed as

$$k_T N_1(p, q) = \phi(p) + \psi(p, q) \quad (24)$$

such that $\psi(p, 0) = 0$. Thus, $\phi(p)$ can be determined using data from the hydrostatic compression phase of CTC experiments. Only the data from the 375 MPa test and the loading part of the 450 MPa cycle of the 500 MPa hydrostatic experiment were utilized. A monotonically increasing function of pressure which tends asymptotically to a constant limiting value (corresponding to fully compacted state)

$$\phi(p) = \phi_0 + \frac{\phi_1}{1 + \exp\left[-\frac{p - \phi_2}{\phi_3}\right]} \quad (25)$$

where $\phi_0 = -7.16 \times 10^{-5}$, $\phi_1 = 0.008$, $\phi_2 = 295.866$ MPa, and $\phi_3 = 62.64$ MPa, approximates the data well. To determine $\psi(p, q)$, Equation (22) along with the data from the deviatoric phase of CTC tests was used. Figure 16 shows the experimental variation of ψ with the principal stress difference (i.e. q) obtained from various CTC tests. Positive ψ values correspond to compressible response, whereas negative ψ values indicate dilatant behavior. Note that for unconfined loading the response is largely dilatant with only very little compressibility at low stress levels. Based on these data, $\psi(p, q)$ was approximated with the function:

$$\psi(p, q) = \begin{cases} \psi_{C_1}(p, q) & \text{for } q \leq \gamma(p, q) \\ \psi_{C_2}(p, q) & \text{for } \gamma(p, q) < q \leq \alpha(p, q) \\ \psi_D(p, q) & \text{for } \alpha(p, q) < q \end{cases} \quad (26)$$

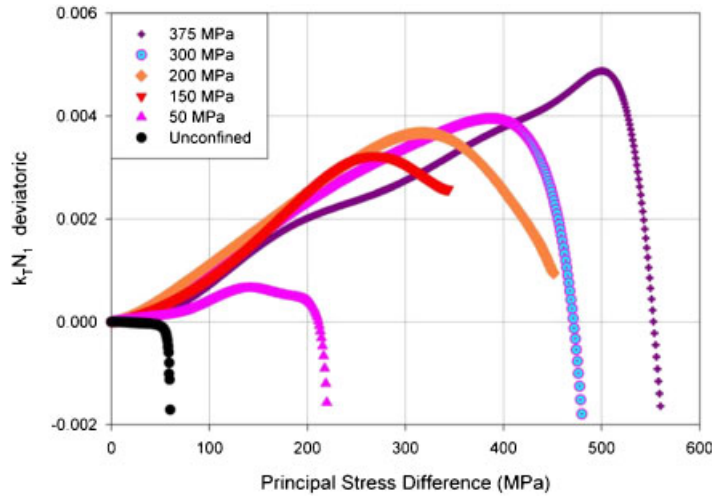


Figure 16. Experimental variation of $k_T N_1$ deviatoric as a function of the principal stress difference q as obtained from different CTC tests.

In the above expression, $\gamma(p, q) = \gamma_0 \sigma_3^{\gamma_1} + \gamma_2$ with $\gamma_0 = 87$, $\gamma_1 = 0.7$, and $\gamma_2 = 1.8$, whereas $\alpha(p, q)$ describes the compressibility/dilatancy boundary. A decaying exponential well approximates this boundary (see Figure 17). Thus,

$$\alpha(p, q) = \alpha_0 + \alpha_1 \left(1 - \exp \left[-\alpha_2 \frac{\sigma_3}{p_a} \right] \right) \quad (27)$$

with $\alpha_0 = 3.6$ MPa, $\alpha_1 = 590.05$ MPa, $\alpha_2 = 0.007$, and $p_a = 1$ MPa is a dimensionalization constant.

The expressions of all the other functions involved in Equation (26) are

$$\psi_{C_1}(p, q) = \beta(p, q) + \psi_1(p, q) \left[1 - \exp \left[-\frac{1}{2} \left(\frac{q - \gamma(p, q)}{\psi_2(p, q)} \right)^2 \right] \right] \quad (28)$$

$$\psi_{C_2}(p, q) = \beta(p, q) \left[\exp \left[-\frac{1}{2} \left(\frac{q - \gamma(p, q)}{\psi_7} \right)^2 \right] - \frac{\exp \left[-\frac{1}{2} \left(\frac{\alpha(p, q) - \gamma(p, q)}{\psi_7} \right)^2 \right]}{1 - \exp \left[-\frac{1}{2} \left(\frac{\alpha(p, q) - \gamma(p, q)}{\psi_7} \right)^2 \right]} \right] \quad (29)$$

and

$$\psi_D(p, q) = \frac{(\psi_{8a} \sigma_3 + \psi_{8b})(q - \alpha(p, q))}{1 - q \left(\frac{\psi_{9a} + \psi_{9b} \sigma_3}{1 + \psi_{9c} \sigma_3} \right)} \quad (30)$$

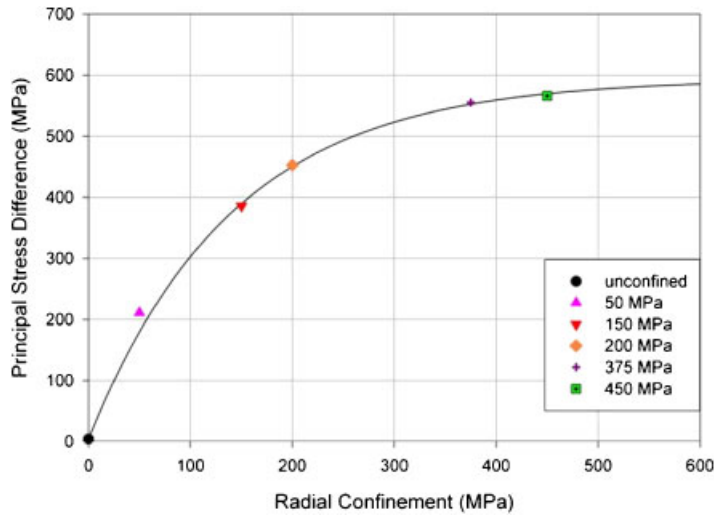


Figure 17. Compressibility/dilatancy boundary for concrete.

with

$$\begin{aligned}\beta(p, q) &= \frac{\beta_0 + \beta_1 \sigma_3}{1 + \beta_2 \sigma_3 / p_a} + \beta_3 \\ \psi_1(p, q) &= \frac{\psi_{1a} + \psi_{1a} \sigma_3 / p_a}{1 + \psi_{1b} \sigma_3} + \psi_{1c} \\ \psi_2(p, q) &= \psi_{2a} \left(\frac{\sigma_3}{p_a} \right)^{\psi_{2b}} + \psi_{2c}\end{aligned}\tag{31}$$

and $\beta_0 = 2 \times 10^{-6}$, $\beta_1 = 3.3 \times 10^{-6}$, $\beta_2 = 0.4$, $\beta_3 = 1.7 \times 10^{-6}$, $\psi_{1a} = 3.3 \times 10^{-6}$, $\psi_{1b} = 0.004$, $\psi_{1c} = 4.38 \times 10^{-6}$, $\psi_{2a} = 1.95$, $\psi_{2b} = 0.8$, and $\psi_{3c} = 13$, $\psi_7 = 5$ GPa, $\psi_{8a} = -1.2 \times 10^{-7}$, $\psi_{8b} = -3.04 \times 10^{-7}$, $\psi_{9a} = 60$, $\psi_{9b} = 4.37$, and $\psi_{9c} = 0.0043$. The only constitutive function yet to be determined is $k_T N_2(p, q)$, which governs the deviatoric irreversible stress-strain response (see Equations (23)). Based on unconfined data and CTC test data at $\sigma_3 = 50, 150$, and 300 MPa, respectively, $k_T N_2(p, q)$ was approximated by

$$k N_2(p, q) = \xi_0 \left(\frac{q}{p_a} \right)^{1.5} + \left(1 - \exp \left[-\frac{q/p_a - \xi_1}{\xi_3} \right] \right) U \left(\frac{q}{p_a} - \xi_1 \right) \left(\frac{q/p_a - \xi_1}{1 - (q/p_a)/\xi_2} \right)\tag{32}$$

All the coefficients involved in Equation (32) are functions of the confining pressure, i.e.

$$\xi_0(\sigma_3) = \xi_0^{(1)} - H \left[\frac{\sigma_3}{p_a} - \xi_{0g} + \xi_{0h} \ln \left(1 - \frac{\sqrt{2}}{2} \right) + \xi_{0c} \right] \cdot \xi_0^{(2)}\tag{33}$$

$$\xi_1(\sigma_3) = \xi_{1a} \exp \left[-\exp \left[-\frac{\sigma_3/p_a - \xi_{1c} \ln(\ln(2)) - \xi_{1b}}{\xi_{1c}} \right] \right]\tag{34}$$

and

$$\xi_2(\sigma_3) = \frac{\xi_{2a} + \xi_{2b} \sigma_3 / p_a}{1 + \xi_{2c} \sigma_3 / p_a}\tag{35}$$

In Equation (32), U is the step function defined as

$$U(x) = \begin{cases} 1 & \text{for } x \geq 0 \\ 0 & \text{for } x < 0 \end{cases}\tag{36}$$

while

$$\xi_0^{(1)}(\sigma_3) = \xi_{0a} + \frac{\xi_{0b}}{(1 + ((\sigma_3 - \xi_{0c})/\xi_{0d})^2)}\tag{37}$$

and

$$\xi_0^{(2)}(p, q) = \xi_{0e} + \xi_{0f} \left(1 - \exp \left[-\frac{\sigma_3 - \xi_{0c} - \xi_{0h} \ln(1 - \sqrt{2}/2) - \xi_{0g}}{\xi_{0h}} \right] \right)^2\tag{38}$$

The coefficients in the above equations are $\xi_{0a} = -2.14 \times 10^{-5}$, $\xi_{0b} = 2.5 \times 10^{-5}$, $\xi_{0c} = 200$, and $\xi_{0d} = 641.51$, $\xi_{0e} = 3.7 \times 10^{-9}$, $\xi_{0f} = -2.14 \times 10^{-5}$, $\xi_{0g} = 612.77$, and $\xi_{0h} = 441.12$, whereas

$\xi_{1a} = 414.1$, $\xi_{1b} = 67.83$, and $\xi_{1c} = 61.03$, $\xi_{2a} = 61.624$, $\xi_{2b} = 2.9$, $\xi_{2c} = 0.00177$, and $\xi_3 = 1881464$. A comparison between calculated and experimental $k_T N_2(p, q)$ corresponding to unconfined loading and $\sigma_3 = 150$ and 375 MPa, respectively, is shown in Figure 18.

Figure 19 shows a comparison between calculated and experimental results for the uniaxial compression case. Note that the model well describes the overall behavior. The volumetric response

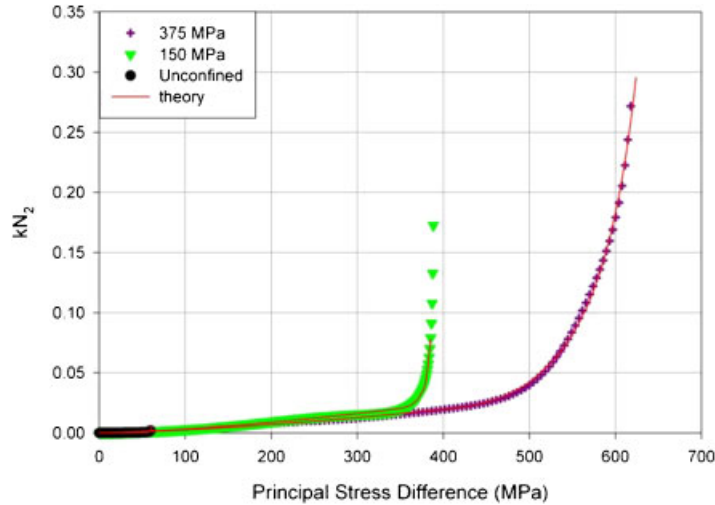


Figure 18. Comparison between experimental and theoretical variations of kN_2 as a function of the principal stress difference for $\sigma_3 = 0, 150$, and 375 MPa.

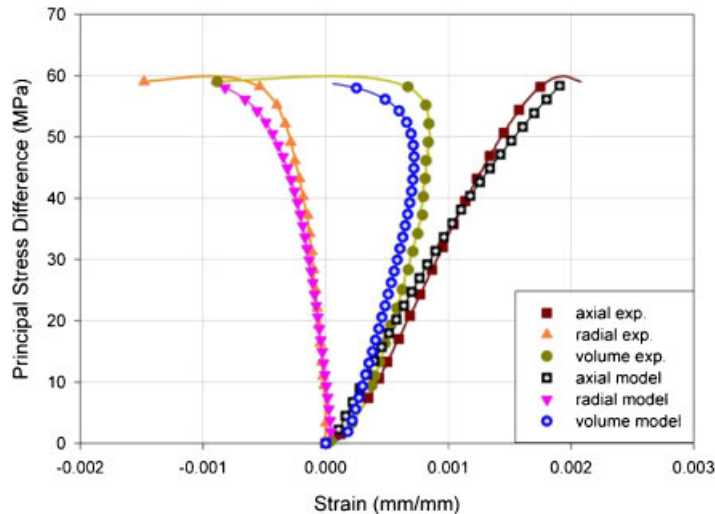


Figure 19. Comparison between simulated and experimental stress–strain responses under uniaxial compression.

as well as the transition from compressibility to dilatancy is particularly well captured. Simulation of the material response under hydrostatic compression is presented in Figure 20. A good correlation between experimental and simulation results is obtained. Finally, we present a comparison between simulation and experimental results for triaxial compression at a confining pressure of 375 MPa. Note that both regimes of the volumetric behavior (i.e. compressibility and dilatancy) are accurately simulated (see Figure 21).

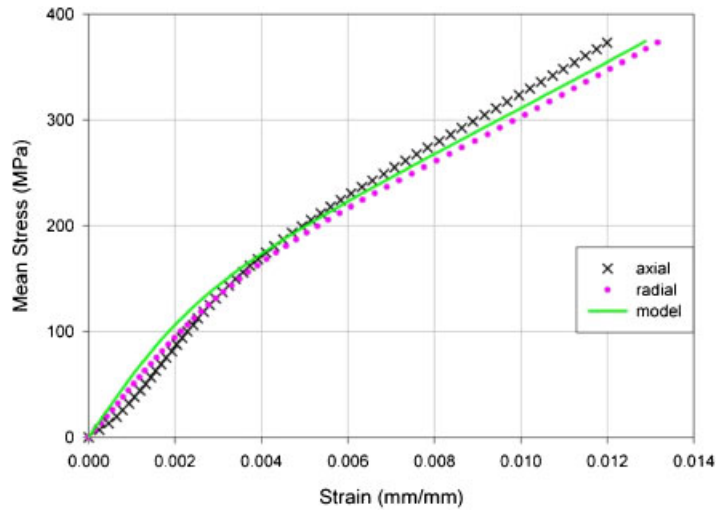


Figure 20. Comparison between theoretical and experimental responses under hydrostatic compression.

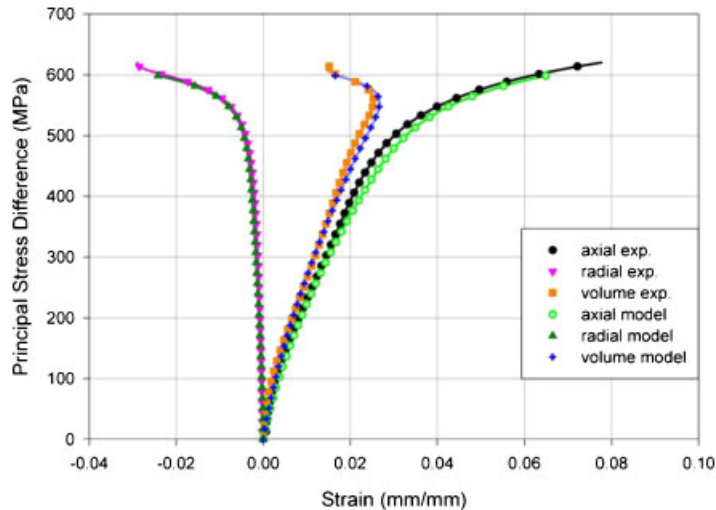


Figure 21. Comparison between theoretical and experimental responses under triaxial compression at a confining pressure of 375 MPa.

4. CONCLUSIONS AND FINAL REMARKS

An experimental investigation into the effects of high confinement on the deformation and strength of a concrete material was conducted. By performing CTC tests with several load–creep–unload and reload cycles, we have determined the elastic parameters with high accuracy. The elastic parameters were found to depend on the stress state. Comparison between the mean stress *vs* volumetric strain data for the deviatoric phase of triaxial compression tests and the data obtained under hydrostatic compression led to the following remarks: (a) for the same level of the mean stress, the compaction (void reduction) under confinement is much higher than under hydrostatic compression and (b) the maximum compaction that can be achieved depends on the confining pressure. It appears that shear influences the compaction mechanisms. Similar conclusions have been reported by Cazacu *et al.* [19] for alumina powder and recently by Burlion *et al.* [25] for a very fine aggregate concrete. As a consequence, the deviatoric and hydrostatic responses cannot be considered to be decoupled. In this paper, we focused on modeling the effect of time (short-term creep) on the plastic response at very high confinement pressures. An elastic/viscoplastic modeling approach was adopted. The expressions of the creep-stabilization boundary, strain-rate orientation tensor (that governs the evolution of the irreversible strain) were determined directly from the experimental data. We compared the model predictions for standard compression tests with data. Good agreement between simulated and experimental response over the full range of confining pressures (up to 0.5 GPa) was obtained. Data for non-monotonic loading in this high-pressure regime were not available. The validity of the model for non-monotonic loadings needs to be further investigated.

APPENDIX: SUMMARY OF THE MODEL PARAMETERS AND CALIBRATION PROCEDURE

Elastic behavior

Young's modulus E

- Determined from the slopes of the quasi-linear parts of the unloading–reloading cycles performed at the end of each of the creep steps in the CTC tests at $\sigma_3 = 300$ and 450 MPa, respectively.
- Parameters involved in the law of evolution of E with mean stress p (see Equations (6)): E^∞ , b , and c .

The Poisson coefficient ν

Hydrostatic yield function $H_h(p)$:

- Calibrated by approximating the variation with mean stress of the irreversible stress work at creep stabilization corresponding to the hydrostatic phase of CTC tests at 150, 300, 450, and 500 MPa confinement, respectively.
- Parameters: a_h , b_h , c_h , d_h , and e_h (see Equations (11)).

Deviatoric yield function $H_d(p, q)$:

- Calibrated by approximating the variation with the principal stress difference q , of W_D (irreversible work associated with irreversible shape change) corresponding to the deviatoric phase of CTC tests at 150, 300, 450, and 500 MPa confinement, respectively.
- Parameters: d_{0_a} , d_{0_b} , d_{1_a} , d_{1_b} , d_{2_a} , d_{2_b} , d_{2_c} , d_{3_a} , and d_{3_b} (see Equations (13)–(15)).

Irreversible volumetric response: $N_1(p, q)$ (see Equations (24))

- Its hydrostatic component, denoted as $\phi(p)$, is calibrated by approximating the variation with mean stress of the experimental irreversible volumetric stain corresponding to the hydrostatic compression phase of CTC experiments at 450 MPa cycle and 500 MPa confinement, respectively. Parameters: ϕ_0 , ϕ_1 , ϕ_2 , and ϕ_3 (see (25)).
- Its deviatoric component, denoted as $\psi(p, q)$, is calibrated by approximating the variation with q of the experimental irreversible volumetric stain corresponding to the deviatoric phase of CTC experiments at 150, 300, 450 MPa cycle and 500 MPa confinement, respectively.
- Parameters: γ_0 , γ_1 , γ_2 , α_0 , α_1 , and α_2 (see (26)–(27)).

Irreversible shear response: $N_2(p, q)$ (see Equations (23))

- Calibrated by approximating the variation with q of the experimental irreversible deviatoric stain corresponding to the deviatoric phase of CTC experiments at 150, 300, 450 and 500 MPa confinement.
- Parameters: ξ_{0a} , ξ_{0b} , ξ_{0c} and ξ_{0d} , ξ_{0e} , ξ_{0f} , ξ_{0g} , ξ_{0h} , ξ_{1a} , ξ_{1b} , ξ_{1c} , ξ_{2a} , ξ_{2b} , ξ_{2c} , and ξ_3 .

REFERENCES

1. Van Mier JGM. Strain softening of concrete under multiaxial loading conditions. *Doctoral Dissertation*, Eindhoven University of Technology, The Netherlands, 1984.
2. Mazars J, Pijaudier-Cabot G. Continuum damage theory: application to concrete. *Journal of Engineering Mechanics* (ASCE) 1989; **115**:345–365.
3. Cristescu N. *Rock Rheology*. Kluwer Academic Publishers: The Netherlands, 1989.
4. Cristescu N, Hunsche U. *Time Effects in Rock Mechanics*. Wiley: England, 1998.
5. Schickert G, Danssman J. Behavior of concrete stressed by high hydrostatic compression. *Proceedings of the International Conference on Concrete under Multiaxial Conditions*, vol. 2. University Paul Sabatier Press: Toulouse, France, 1984; 9–19.
6. Bazant ZP, Bishop FC, Chang TP. Confined compression test of cement paste and concrete up to 300 Ksi. *ACI Journal* 1986; **33**:553–560.
7. Bourlion N, Pijaudier-Cabot G, Dahan N. Experimental analysis of compaction of concrete and mortar. *International Journal for Numerical and Analytical Methods in Geomechanics* 2001; **25**:1467–1486.
8. Krajcinovic D. *Damage Mechanics*. North-Holland Series in Applied Mathematics and Mechanics. Elsevier: Amsterdam, 1996.
9. Skrzypek J, Ganczarski A. *Modeling of Material Damage and Failure of Structures: Theory and Applications*. Springer: Berlin, Heidelberg, New York, 1999.
10. Yang BL, Dafalias YF, Hermann LR. A bounding surface plasticity model for concrete. *Journal of Engineering Mechanics* (ASCE) 1985; **111**:359–380.
11. Este G, Willam K. Fracture energy formulation for inelastic behavior of plain concrete. *Journal of Engineering Mechanics* (ASCE) 1994; **120**:1983–2011.
12. Ortiz M. A constitutive theory for the inelastic behavior of concrete. *Mechanics of Materials* 1985; **4**:67–93.
13. Simo JC, Ju JW. Relative displacement and stress based continuum damage models. I: formulation. *International Journal of Solids and Structures* 1987; **23**:821–840.
14. Abu-Lebeh M, Voyadjis GZ. Plasticity-damage model for concrete under cyclic multiaxial loading. *Journal of Engineering Mechanics* (ASCE) 1993; **119**:1465–1484.
15. Ekh M, Runesson K. Bifurcation results for plasticity coupled to damage with MCR-effect. *International Journal of Solids and Structures* 2000; **37**:1975–1996.
16. Halm D, Dragon A. An anisotropic model of damage and frictional sliding for brittle materials. *European Journal of Mechanics – A/Solids* 1998; **17**:439–460.
17. Perzyna P. Fundamental problems in viscoplasticity. *Advances in Applied Mechanics* 1966; **9**:243–377.
18. Katona MG. Evaluation of viscoplastic Cap model. *Journal of Geotechnical Engineering* (ASCE) 1984; **110**: 1106–1125.

CHARACTERIZING THE BEHAVIOR OF CONCRETE

19. Cazacu O, Jin J, Cristescu ND. A new constitutive model for alumina powder compaction. *KONA Powder and Particle* 1997; **15**:103–112.
20. Truesdell C. Hypoelasticity. *Journal of Rational Mechanics and Analysis* 1955; **4**:83–133.
21. Loret B. On the choice of elastic parameters for sand. *International Journal for Numerical and Analytical Methods in Geomechanics* 1985; **9**:285–292.
22. Neville AM. *Properties of Concrete*. Wiley: New York, 1973.
23. Wilbeck JS. Classification of impact regimes. *Technical Report SwRI Project 06-9304*, South West Research Institute, San Antonio, TX, 1985.
24. Wang CC. A new representation theorem for isotropic functions, Part I and II. *Archive for Rational Mechanics and Analysis* 1970; **36**:166–223.
25. Burlion N, Pijaudier-Cabot G, Dahan N. Experimental analysis of compaction of concrete and mortar. *International Journal for Numerical and Analytical Methods in Geomechanics* 2001; **25**(15):1467–1486.